Plasma-sprayed thermal barrier coatings: numerical study on damage localization and evolution

K. Slámečka, P. Skalka, L. Čelko, J. Pokluda

Brno University of Technology, Central European Institute of Technology, Technická 10, 616 69 Brno, Czech Republic
k.slamecka@ceitec.vutbr.cz, p.skalka@ceitec.vutbr.cz, l.celko@ceitec.vutbr.cz, j.pokluda@ceitec.vutbr.cz

L. Saucedo-Mora, T. J. Marrow

University of Oxford, Department of Materials, Parks Road, Oxford OX1 3PH, UK
luis.saucedomora@materials.ox.ac.uk, james.marrow@materials.ox.ac.uk

U. Thandavamoorthy

Ecole des Mines de Nantes, 4 Rue Alfred Kastler, 44300 Nantes, France
t_uma@hotmail.fr

ABSTRACT. Thermal barrier coatings (TBCs) are advanced material systems used to enhance performance and in-service life of components operated at high temperatures in gas turbines and other power-generation devices. Because of complexity, numerical methods became important tools both for design of these coatings and for in-service life estimations and optimization. In this contribution, two main features that affect the TBCs' performance, namely the roughness of the bond coat and the microstructure of the ceramic top coat, are discussed based on Finite Element Method (FEM) and Finite Element Microstructure MEshfree (FEMME) simulations that were used to calculate stresses and assess damage within the coating. Roughness data obtained from plasma-sprayed CoNiCrAlY + YSZ coated samples are supplemented to discuss assumptions and results of employed numerical models.

KEYWORDS. Thermal barrier coatings; Plasma spraying; Finite element modelling; Multi-scale numerical model; Roughness.

INTRODUCTION

T hermal barrier coatings (TBCs) are advanced material systems used to enhance performance and in-service life of components operated at high temperatures in gas turbines and other power-generation devices [1]. TBCs usually consist of two applied layers: (i) an aluminium-rich metallic bond coat (BC), and (ii) an yttria-stabilized zirconia (YSZ) insulating ceramic top coat (TC), Fig. 1. The third thin oxide layer (the so-called thermally grown oxide – TGO) gradually develops at high temperatures at the TC/BC interface, thus resulting in a three-layer system. The main failure mode of TBCs is spallation of the top coat resulting from damage accumulated at or near the TC/BC interface that is followed by rapid deterioration of properties of the bond coat and the load-bearing superalloy substrate. In the case of TBCs prepared by plasma spraying, coating spallation is due to propagation and coalescence of cracks that are nucleated at

microstructural imperfections within the top coat, the TGO or at either of its interfaces, according to the relative importance of the misfit stresses experienced upon cooling, the TGO-growth stresses building up during high-temperature exposure and counteracting stress-relaxation processes such as high-temperature creep or sintering of the top coat [2, 3].
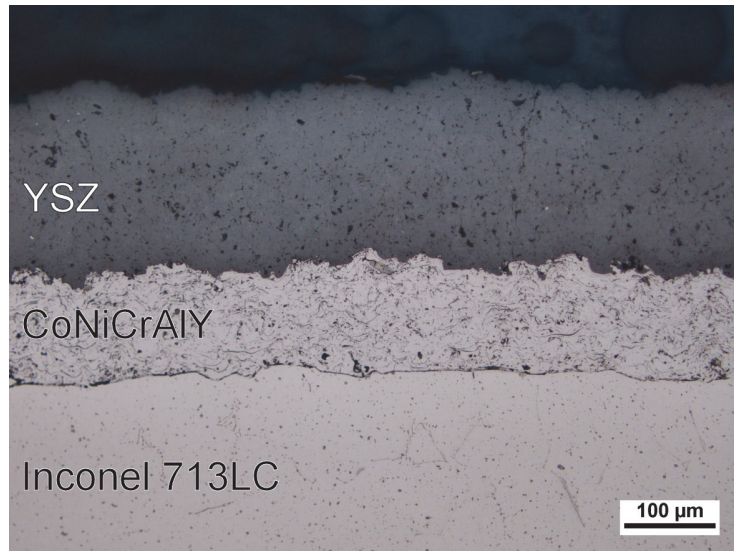

Figure 1: Atmospheric-plasma-sprayed CoNiCrAlY + YSZ thermal barrier coating on Inconel 713 LC substrate.

One of the key features significantly influencing the damage development is the "roughness" (or more precisely the "surface texture" or "surface topography") of the bond coat. The roughness affects the oxidation of the bond coat (i.e. the growth of the TGO layer) and the initial as-sprayed microstructure of the top coat (and hence the overall stiffness of the top coat and also the availability of easy-growth crack paths near the interface) [4] thus governing the nature and evolution of stresses and strains and the actual coating failure mode. The modification of the interfacial roughness as a means of enhancing the coating lifetime has been exploited by several authors, e.g. [5-7]. Nowadays, it is agreed that a certain level of bond coat roughness is needed, as top coat bonding is provided primarily via mechanical interlocking, but that too rough coatings would fail prematurely. Experimental studies performed by Liu et al. [4], Dong et al. [5] and Chen et al. [8] also indicate that understanding the relationship between the "type" of roughness and the near-interface TC microstructure could be important in answering on what technological modifications of the bond coat prior to spraying of the top coat are desirable to maximize the performance. Given the complexity of the TBC systems and their operational modes, numerical methods have become important tools both for design of these coatings and for in-service life estimations and optimization. Present models allow the inclusion of many aspects of the degradation process, such as the creep deformation of individual constituents, the actual growth of the TGO layer, or sintering of the ceramic top coat, but they are usually restricted to two-dimensional problems and the continuum representation of the top coat as the realistic modelling of any intricate irregular topography and/or multiple material microstructural defects can impose enormous computational costs. In this contribution, the effect of these two features on stresses in critical locations (the top coat and the interfaces between the top coat, TGO, and the bond coat) and on damage evolution is discu   ssed based on Finite Element (FE) and advanced Finite Element Microstructure MEshfree (FEMME) [9] calculations. The performed simulations point to the necessity of incorporating a realistic representation of roughness/microstructure into further studies on possible TBCs lifetime improvements.

NUMERICAL MODELLING

F E calculations on a TBC with an irregular TC/BC interface were done using FE software ANSYS (ANSYS, Inc., Canonsburg, USA). The multilayer infinite-plate model consisted of (i) a nickel-base superalloy substrate, (ii) a generic MCrAlY bond coat, (iii) a single continuous α-alumina TGO layer, and (iv) an YSZ top coat having the following thicknesses: $t_{substrate}$ = 25 mm, t_{BC} = t_{TC} = 200 μm and t_{TGO} = 0 and 3 μm (the intermediate stable growing state). All layers were assumed to be isotropic homogeneous materials with the ideal elastic (substrate, TGO, TC) or the

elastic-ideally plastic (BC) behavior. Material properties were obtained from references [10, 11] and the in-house database and they reflect the internal porosity of the YSZ top coat (the stiffness of 15 GPa is assumed being more than an order of magnitude smaller than the Young's modulus of dense YSZ of 210 GPa).

The geometry of the TC/BC interface was modelled based on profilometric measurements of a plasma-sprayed YSZ top coat [12]. The residual data were obtained after subtracting the specimen's circular shape and were then decomposed into the roughness and the waviness components by using a Gaussian filter with an arbitrarily chosen cut-off wavelength of 200 μm. The waviness data of approximately 1 mm² in size were used for FE calculations in order to alleviate the demands on CPU power and to diminish the differences between the topographies of TC and BC that are caused mostly by differences in material (ceramic, metal) and powder feedstock properties. Indeed, while the roughness of the bond coat and the top coat, as quantified by the average roughness S_a (the average absolute deviation of roughness irregularities from the mean plane), the root mean square roughness S_q (the standard deviation of the distribution of height z-coordinates), and the surface roughness R_S (a ratio of the "true" and the projected surface area), is considerably different, the waviness in both cases is reasonably similar, Tab. 1. The simulated thermal loading consisted of a single cooling step from a temperature of 1020 °C at which a stress-free state was assumed in all materials. The system was isothermally cooled down to room temperature and the stresses at critical locations (YSZ and interfaces between YSZ, TGO, and BC) were studied.
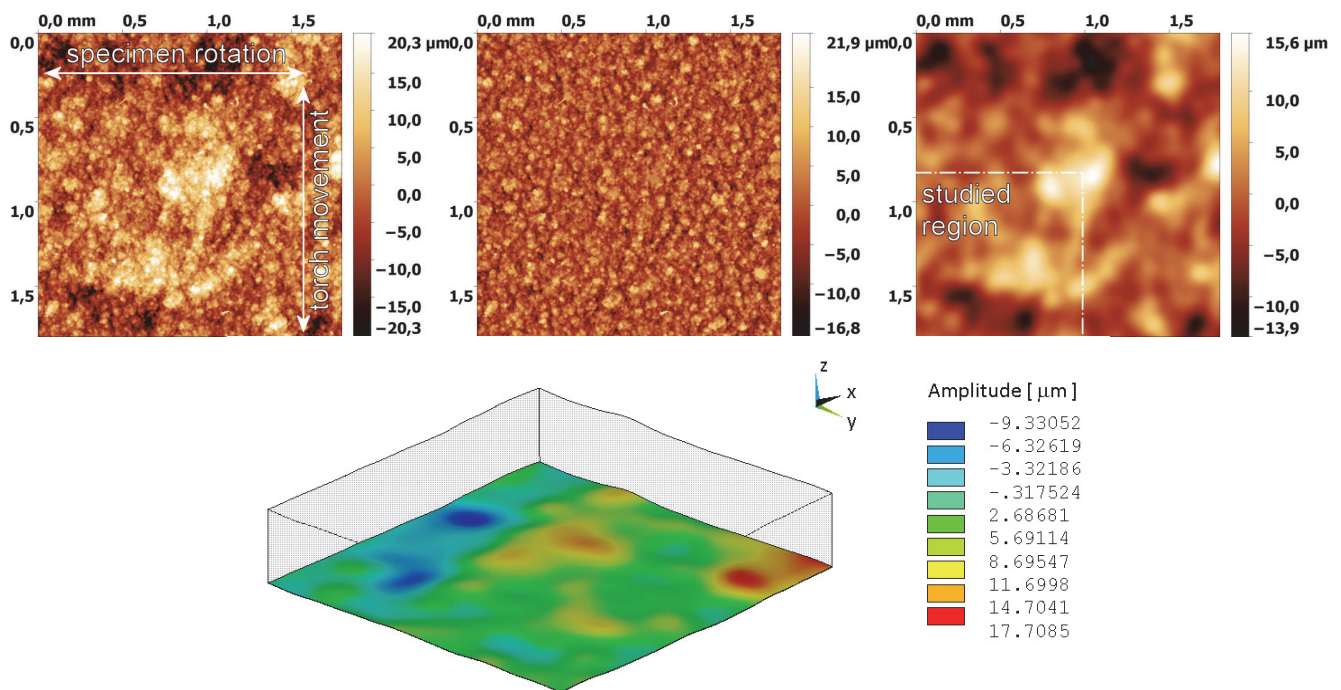

Figure 2: Residual surface data (top left) of the as-sprayed YSZ top coat, its decomposition into the roughness (top middle) and waviness (top right) components, and rendering of the studied part of waviness data in ANSYS (bottom).

	Parameters (BC/TC)		
Data	S_a (μm)	S_q (μm)	R_S (−)
Residual	8.7/5.5	11.0/6.9	1.82/1.28
Roughness	6.3/3.3	8.0/4.2	1.82/1.28
Waviness	4.8/3.8	6.1/5.0	1.01/1.00

Table 1: Comparison of the topographical parameters obtained for the as-sprayed CoNiCrAlY bond coat and YSZ top coat.

The FEMME [9] (Finite Elements Microstructure MEshfree) method allows one to describe a complex graded microstructure, using a Cellular Automata (CA) model, with a generic FEM (Finite Element Model with irregular

tetrahedrons) to simulate complex sample geometries, with computational efficiency. In order to model quasi-brittle fracture in materials with a complex microstructure, we insert variations in its discretization and the relationship between the CA and FE layers through the introduction of a Meshfree framework as further layer between them. The versatility of the Meshfree framework allows us to connect variable domains with different geometries and numbers of nodes. Each layer defines a different size scale and is solved with a different method. For the large size scale macromechanical layer a standard, relatively coarse, finite element model is used. In the small size scale layer we use a cellular automata method, where the different cells represent the properties of the quasi-brittle material. A Microstructural Adaptive Meshfree (MAM) framework has been developed to solve the displacements of the microstructural features in the intermediate layer. The Meshfree model uses the microstructural features as its discretization, dividing the microstructure into Particle Domains (PD) that represent each particle with a single domain, and Inter Particle Domains (IPD) that link the particles and represent the matrix, Fig. 3. From the large scale downwards to the small scale the information is shared between layers by the displacements, which provide the boundary conditions. From the small scale upwards to the larger scale the information is shared by the energy homogenization of the damage in the material to link the effects of the eroded (i.e. damaged) cells of the CA with the FE behavior [13].
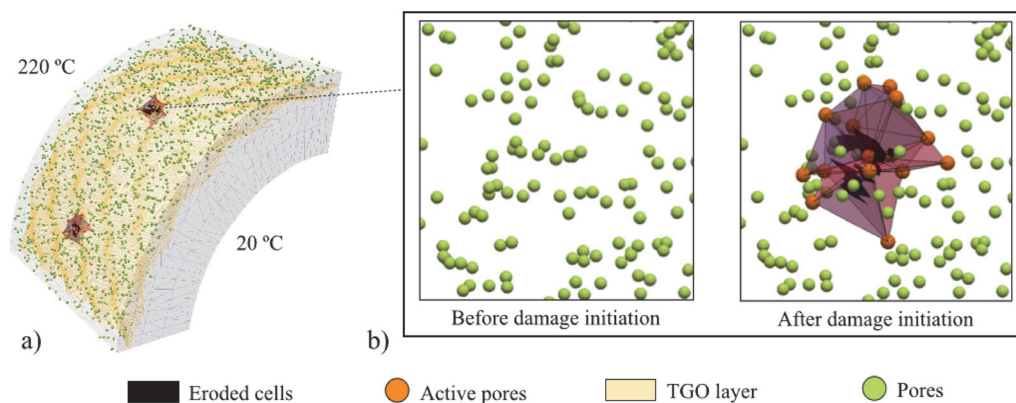

Figure 3: Detail of the different layers of the FEMME model (i.e.: FE mesh, IPD, pores and eroded cells), and the local initiation of the damage.

The aim is to evaluate the influence of the fully developed TGO layer geometry on the development of damage in the TBC system deposited on a tube with an internal radius of 3.5 mm, outer radius of 5.53 mm and length of 5 mm. The modeled system consists of a nickel base superalloy single crystal CMSX-4 substrate, MCrAlY bond coat and YSZ top coat with temperature dependent material properties obtained from reference [14]. The effect of a quasi-static increase in the external temperature, with constant internal temperature (20°C), was simulated. The thicknesses are 1.5 mm for the metallic substrate, 150 μm for the BC, 8 μm for the TGO and 300 μm for the top coat. The TGO interface geometry is defined using a three-dimensional sine wave with amplitude (A) and wavelength (λ) with A/λ of 0.32: i.e. $\lambda = 314$ μm and $A = 100$ μm. These parameters permit a good quality FE mesh with reasonable computational cost, although due to this current limitation, the model represents, as in the FE calculations, only the waviness surface component. The ratio A/λ, rather than the amplitude A itself, is expected to be the dominant factor affecting the magnitude of stresses developed due to anisotropic volume changes related to the TGO growth at high temperatures and also the stresses developed due to different coefficients of thermal expansion upon cooling; in both cases the stresses have been reported to increase with increasing interfacial roughness.

RESULTS AND DISCUSSION

Evolution of stresses in TBC due to irregular YSZ/BC interface

The YSZ/BC interface represents the critical location where damage ultimately always occurs because of the presence of growing TGO layer. As evidenced by internal cracks within the TGO that follow the traces of earlier interfacial separations, the ceramic/metallic interface between the TGO and the bond coat is more susceptible to cracking [15]. The magnitudes of normal stresses at this interface increases with increasing thickness of the TGO layer,

Fig. 4. The initial stresses follow the waviness of the surface with tensile stresses (i.e. the negative contact pressure) located at the bond coat peaks and compressive stresses located in the valleys. When the TGO of the thickness of 3 μm is introduced, not only do the magnitudes of these stresses increase but they are also redistributed and the correlation with the surface topography and the initial stress state is significantly diminished, Fig. 4. Such evolution corresponds to the stress conversion, the onset of which depends on the local geometry of the interface [5, 11, 16]. The TGO layer is nearly under biaxial compression with the first principal stress σ_1 being negligible, and with the second and third principal stresses being predicted to be approximately -2.6 GPa, Fig. 5. Given the compressive strength of alumina of 2-4 GPa, the waviness by itself might at this stage induce local cracking of the TGO during the cooling part of the cycle, if it is not counteracted by sufficient creep stress relaxation at high temperatures.
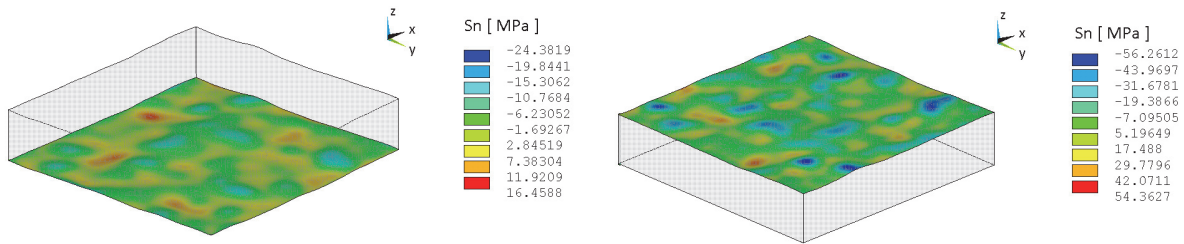

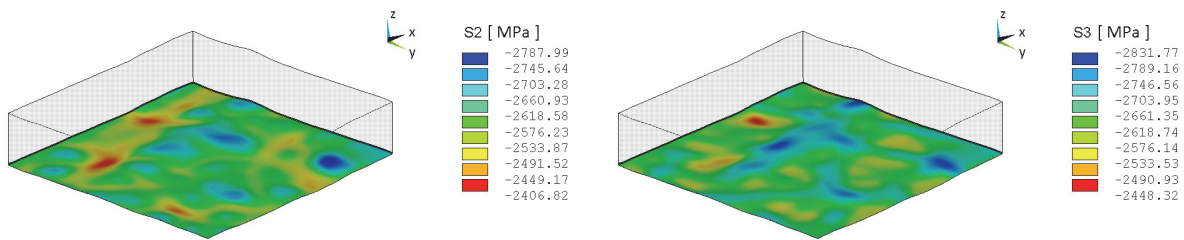Figure 4: Contact pressure at the TGO/BC interface for $t_{TGO} = 0$ μm (left), and $t_{TGO} = 3$ μm (right).

Figure 5: The principal stresses σ_2, σ_3 in the TGO layer ($t_{TGO} = 3$ μm).

The stresses in the top coat, which are essential when the loading involves fast thermal cycling and the failure occurs due to delamination cracks initiated at microstructural defects such as pores or de-bonded splat boundaries, initially decrease with BC oxidation, Figs. 6, 7. The highest tensile stresses are located near the bond coat peaks. The correlation with local interfacial features remains high when the TGO layer is present, the broadening of the tensile regions due to the stress conversion (from tensile to compressive above the peaks and from compressive to tensile above the valleys) is, however, already observed, Fig. 6. Previous calculations on regular surfaces revealed that for the TGO of thickness of 3 μm, the surface with the wavelength of $\lambda = 125$ μm and the amplitude of $A = 10$-30 μm exhibits substantial shift of the tensile region towards the valley, while for the surfaces of $\lambda = 500$ μm, the tensile stresses are still located above the BC peaks [16]. Moreover, with further oxidation, the tensile stresses generally increase and the microcracks formerly arrested in the compression zone above the valleys can continue to propagate and interconnect to form larger delamination cracks leading to the final failure [5].
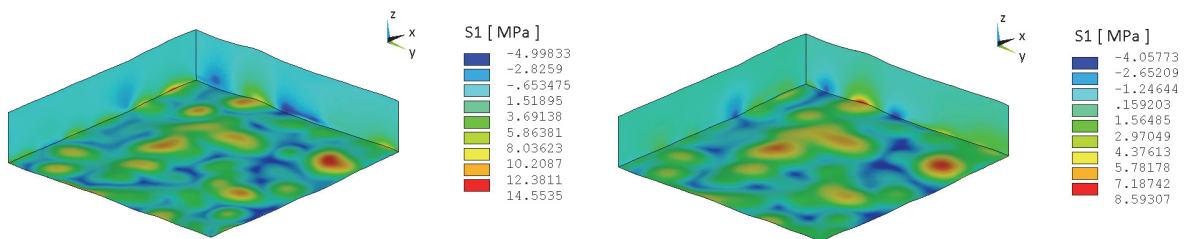

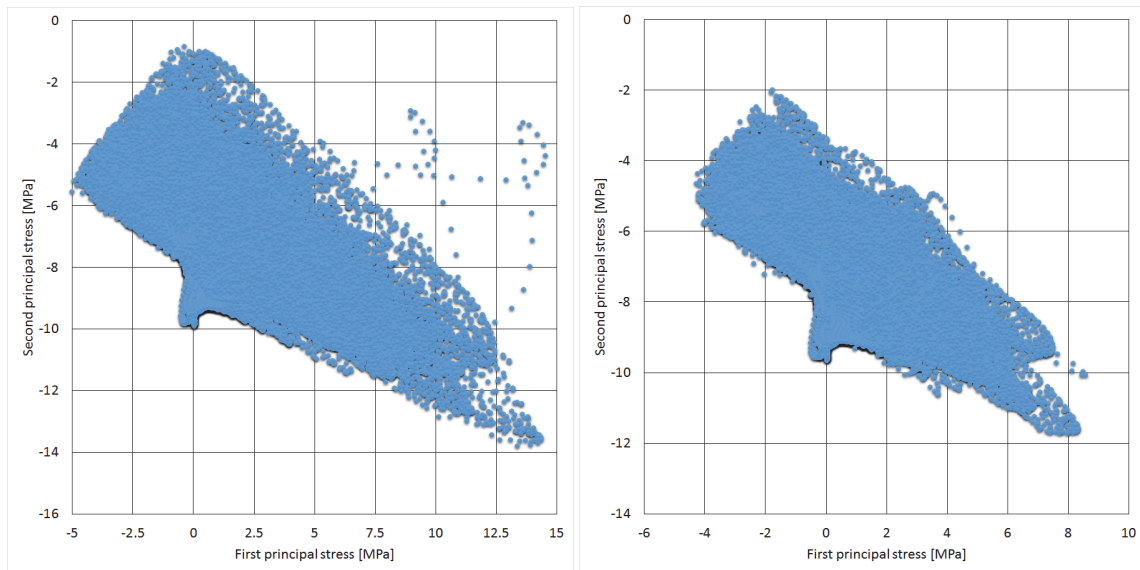Figure 6: The first principal stress σ_1 in the top coat for $t_{TGO} = 0$ μm (left) and $t_{TGO} = 3$ μm (right).

Figure 7: The stress state (σ_1, σ_2) in the top coat for $t_{TGO} = 0$ μm (left) and $t_{TGO} = 3$ μm (right) in all nodes of the YSZ top coat. The third principal stress, σ_3, is compressive in the whole YSZ layer.

Incorporating Microstructure and Damage evolution – FEMME

The damage, which affects the thermal conductivity, has an influence on the temperature of the TC and substrate. To evaluate this, the temperature in each of the finite elements is computed as the average of the temperature in its nodes; this is illustrated in Fig. 8, which shows the variation of the average temperature at two points, on either side of the TGO layer, that are the same distance (5 mm) from the center of the tube. With this we evaluate points under and above the TGO layer. The damage is calculated as an average, from the point analyzed to the surface, of the ratios between the current Young modulus of each element (this reflects erosion of CA cells) and its original values.
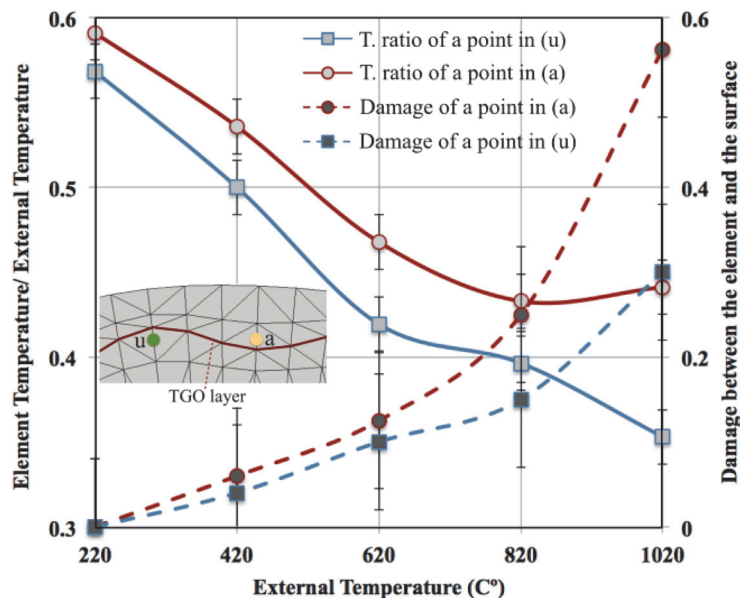

Figure 8: The relationship of the element temperature and damage to the external temperature, at a two points on either side of the TGO layer that are both a distance of 5 mm from the tube center.

The element temperatures are lower than the external temperature due to the low thermal conductivity of the top coat. This is clearly affected by the damage evolution, as the relationship exhibits two regions of different slope; the region at lower external temperature is associated with fractures propagating through the TGO layer, while the region at higher temperature is associated with fracture propagating from the TGO layer to the external surface. Up to 820 ℃ the

temperature decay and the damage growth are approximately linear with external temperature change, and between 820 ºC and 1020 ºC the temperature of the points above the TGO layer increases due to the increment of the damage between those points and the external surface. Up to 820 ºC the damage is developed along the TGO layer, Fig. 8, increasing the insulation of those points, which is shown in the decay of the temperature ratio. Between 820 ºC and 1020 ºC the damage propagates to reach the surface, reducing the insulation and increasing the element temperature relative to the external temperature. The boundary conditions are applied only in the external nodes, so the insulating effect of damage on the conductivity of the damaged finite element is apparent. To model the hotspots created by the cracks in a more representative manner, more complex boundary conditions could be implemented to address the penetration of hot gases through the open cracks.

CONCLUSIONS

The performed calculations show that both the waviness of the BC/TC interface and the microstructure of the ceramic top coat have a significant impact on predicted stresses and the damage evolution. The stresses due to waviness are superimposed with stresses due to the form and with those locally induced by roughness, increasing the chances of an early damage formation near the large BC peaks. The particular crack path is strongly influenced by thermal history, the local waviness and the microstructure of the top coat. A system approach to TBC design and performance improvements thus clearly requires that a realistic representation of both the interfacial geometry and the microstructure is introduced into numerical models.

ACKNOWLEDGEMENTS

REFERENCES

[1] Besmann, T., Interface science of thermal barrier coatings, J. Mater. Sci., 44 (2009) 1661-1663. DOI: 10.1007/s10853-009-3323-0.

[2] Rabiei, A., Evans, A., Failure mechanisms associated with the thermally grown oxide in plasma-sprayed thermal barrier coatings, Acta mater., 48 (2000) 3963-3976. DOI: 10.1007/s10853-009-3323-0.

[3] Evans, A.G., Mumm, D.R., Hutchinson, J.W., Meier, G.H., Pettit, F.S., Mechanisms controlling the durability of thermal barrier coatings, Prog. Mater Sci., 46 (2001) 505-553.

[4] Liu, D., Seraffon, M., Flewitt, P., Simms, N., Nicholls, J., Rickerby, D., Effect of substrate curvature on residual stresses and failure modes of an air plasma sprayed thermal barrier coating system, J. Eur. Ceram. Soc., 33 (2013) 3345-3357. DOI: 10.1016/j.jeurceramsoc.2013.05.018.

[5] Vaßen, R., Kerhoff, G., Stöver, D., Development of a micromechanical life prediction model for plasma sprayed thermal barrier coatings, Mater. Sci. Eng., A303 (2001) 100-109.

[6] Eriksson, R., Sjöström, S., Brodin, H., Johansson, S., Östergrenc, L., Li, X., TBC bond coat–top coat interface roughness: Influence on fatigue life and modelling aspects. Surf. Coat. Technol., 236 (2013) 230-238. DOI: 10.1016/j.surfcoat.2013.09.051.

[7] Dong, S., Song, B., Zhou, G., Hansz, B., Liao, H., Coddet, Ch., Multi-layered thermal barrier coatings fabricated by plasma-spraying and dry-ice blasting: Microstructure characterization and prolonged lifetime, Surf. Coat. Technol., 236 (2013) 557-567. DOI: 10.1016/j.surfcoat.2013.10.066.

[8] Chen, W., Wu, X., Marple, B., Lima, R., Patnaik, P., Pre-oxidation and TGO growth behaviour of an air-plasma-sprayed thermal barrier coating. Surf. Coat. Technol., 202 (2008) 3787-3796. DOI: 10.1016/j.surfcoat.2008.01.021.

[9] Saucedo-Mora, L., Marrow, T.J., Method for the explicit insertion of microstructure in Cellular Automata Finite Element (CAFE) models based on an irregular tetrahedral Finite Element mesh: Application in a multi-scale Finite Element Microstructure MEshfree framework (FEMME), Finite Elem. Anal. Des., 105 (2015) 56-62. DOI: 10.1016/j.finel.2015.07.001

[10] Jahed, H., Shirazi, R., Loading and unloading behavior of a thermoplastic disc, Int. J. Press. Vessels Pip., 78 (2001) 637-645.

[11] Białas, M., Finite element analysis of stress distribution in thermal barrier coatings, Surf. Coat. Technol., 202 (2008) 6002-6010. DOI: 10.1016/j.surfcoat.2008.06.178.

[12] Slámečka, K., Čelko, L., Skalka, P., Pokluda, J., Němec, K., Juliš, M., Klakurková, L., Švejcar, J., Bending fatigue failure of atmospheric-plasma-sprayed CoNiCrAlY+YSZ thermal barrier coatings, Int. J. Fatigue, 70 (2015) 186-195. DOI: 10.1016/j.ijfatigue.2014.09.009.

[13] Hill, R, On the micro-macro transition in constitutive analysis of elastoplastic response at finite strain. Math. Proc. Camb. Phil. Soc., 98 (1985) 579–585. DOI: 10.1017/S0305004100063787.

[14] Bednarz, P., Herzog, R., Trunova, O., Steinbrech, R.W., Echsler, H., Quadakkers, W.J., Schubert, F., Singheiser, L., in D. Zhu, K. Plucknett (Eds.), Proceedings of 29th International Conference on Advanced Ceramics and Composites, Cocoa Beach, USA, (2005) 73-80.

[15] Schlichting, K., Padture, N., Jordan, E., Gell., M., Failure modes in plasma-sprayed thermal barrier coatings. Mater. Sci. Eng., A342 (2003) 120-130.

[16] Skalka, P., Slámečka, K., Pokluda, J., Čelko, L., Stability of plasma-sprayed thermal barrier coatings: the role of the waviness of the bond coat and the thickness of the thermally grown oxide layer, Surf. Coat. Technol., 274 (2015) 26-36. DOI: 10.1016/j.surfcoat.2015.04.021.